Available online at www.sciencedirect.com
ScienceDirect
Journal of Nuclear Materials 375 (2008) 283–289
journal of nuclear materials
www.elsevier.com/locate/jnucmat

Probabilistic failure analysis of a water-cooled tungsten divertor: Impact of embrittlement

J.-H. You *, I. Komarova [1]

Max-Planck-Institut für Plasmaphysik, EURATOM Association, Boltzmannstr. 2, 85748 Garching, Germany

Received 2 August 2007

Abstract

Inherent brittleness and neutron embrittlement are critical weaknesses of tungsten for fusion application. Pronounced scattering of the fracture strength of tungsten requires a statistical treatment. Thus, the risk of structural failure of a tungsten component can be estimated only in a probabilistic framework. In this work, we applied a probabilistic failure analysis code STAU to estimate the failure risk of a water-cooled tungsten mono-block divertor component. The STAU code was based on the weakest-link failure theory and linear elastic fracture mechanics. A typical heat flux load being expected for a fusion reactor was considered for the FEM stress analysis. The failure probability was computed considering various mixed-mode fracture criteria. Both the experimentally estimated and hypothetical Weibull parameters were used as material data. In the case of unirradiated tungsten, the failure probability was acceptably small whereas reduced Weibull parameters led to significantly increased failure risk.

1. Introduction

Tungsten is currently considered as the most favoured armour material for the plasma-facing components (PFC) of fusion reactors. This is due to the unique characteristics of tungsten, particularly such as refractory nature, low sputtering erosion, high strength, reasonable thermal conductivity and acceptable activation [1,2]. On the other hand, low fracture toughness is a critical weakness of most up-to-date tungsten alloys developed for PFC [3]. The toughness problem becomes even more acute during nuclear fusion operation due to the embrittlement caused by neutron irradiation and by recrystallisation [2]. Hence, design of a tungsten PFC for power reactors has to take the potential risk of the embrittlement into account.

The direct consequence of the neutron embrittlement is loss of ductility and toughness. Furthermore, it also imposes a strong impact on the fracture mechanical assessment of structural reliability, because the scattering of strength data requires statistical treatment. Thus, the risk of structural failure of a tungsten PFC can be reasonably estimated only in a probabilistic framework. This fact means that brittleness of a tungsten PFC is not only a metallurgical issue but also an issue of fracture mechanical failure analysis.

In this work, we applied a computation code of FEM-based probabilistic failure analysis to a tungsten PFC subjected to typical heat flux load expected in a fusion power plant. A water-cooled mono-block type PFC was investigated. The probabilistic formulation of failure was based on the weakest-link failure theory. Failure probability was calculated in terms of the Weibull statistics and the linear elastic fracture mechanics (LEFM)

This article consists of two parts. In the first section, experimental results obtained from an unirradiated tungsten plate are presented to demonstrate the basic features. Results from various mixed-mode fracture criteria are compared. In the second section, a parametric study is presented using hypothetical Weibull parameters to show the correlations between data scattering, strength and failure behaviour.

* Corresponding author. Tel.: +49 89 3299 1373.
E-mail address: you@ipp.mpg.de (J.-H. You).
[1] Present address: Institut für Mechanik, Universität Stuttgart, Pfaffenwaldring 7, 70569 Stuttgart, Germany.

0022-3115/$ - see front matter © 2008 Elsevier B.V. All rights reserved.
doi:10.1016/j.jnucmat.2008.01.009

2. FEM model

2.1. Geometry, mesh and materials

The model PFC considered for the FEM study was a water-cooled tungsten mono-block duplex structure consisting of a tungsten armour plate and a CuCrZr alloy cooling tube (heat sink). Mesh and constituent materials of the considered model PFC are illustrated in Fig. 1 for the symmetric half. The reference of this model was the water-cooled divertor design of the European Power Plant Conceptual Study (PPCS model A, WCLL) [4]. The single mono-block armour plate had a dimension of $19.5 \times 18 \times 4\ mm^3$. The heat sink tube had a thickness of 1.5 mm and an inner diameter of 10 mm. The distance from the top surface to the tube was 4.5 mm. The commercial FEM code ABAQUS was employed for the simulation [5]. Quadratic reduced integration continuum elements were used. The displacement of the edge cross-sections of the coolant tube and of the interlayer were fully constrained in the tube axis direction.

A precipitation-hardened CuCrZr alloy was considered for the heat sink tube and a cross-rolled stress-relieved tungsten for the armour block, respectively. The rolled plane was assumed to be oriented perpendicular to the tube axis. For simplicity, tungsten was assumed to be elastically isotropic, which is of course an approximation for a rolled sheet. Temperature-dependent material data were used. Selected material properties are listed in Table 1 [6]. The fully elasto-plastic FEM analysis showed that no plastic yielding occurred in the tungsten block. This result justifies the application of the weakest-link failure theory based on the LEFM.

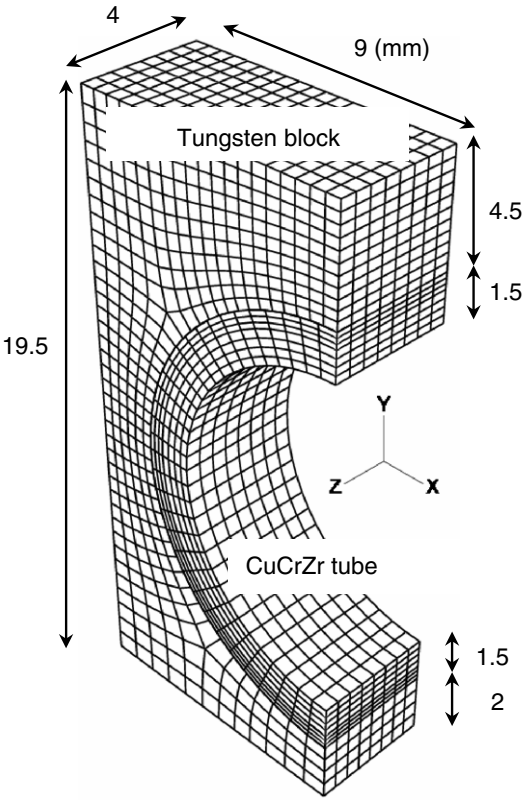

Fig. 1. Finite element mesh of the mono-block divertor model. Only the symmetric left half part was modelled. The reference of this model was the water-cooled divertor design of the PPCS model A (WCLL) [4].

Table 1
Used material properties (reference IMPH) [6]

	W (20 °C)	W (400 °C)	CuCrZr (20 °C)	CuCrZr (400 °C)
Young modulus (GPa)	398	393	128	110
Yield stress (MPa)	1385	948	301	273
CTE (10^{-6}/K)	4.5	4.6	15.5	19.3
Thermal conductivity (W/mK)	175	140	379	352

2.2. Thermal load history

The thermal history of the model PFC considered for simulation includes fabrication process, HHF load cycle and cooling phase. The stress-free temperature was assumed to be 500 °C. The effective stress-free temperature is usually lower than the joining temperature. The initial temperature change was uniform cooling from the stress-free temperature to room temperature. Subsequently, high heat flux loading was simulated assuming a surface heat flux load of 15 MW/m^2 and a volumetric heating load of 0.027 MW/m^3. The temperature and the pressure of the coolant water was 320 °C and 15.5 MPa, respectively. The assumed heat transfer coefficient was 0.156 $MW/m^2\,K$. These parameters correspond to the loading conditions defined for the PPCS Model A power reactor [4].

3. Probabilistic failure analysis

In this work the probabilistic failure analysis code STAU was used [7]. This code was developed as a post-processor for FEM codes from which stress data at individual integration points were imported into STAU for further probabilistic failure computation. STAU consisted of a main processor, an interface programme for a specific FEM code and a data input file.

In STAU the probabilistic description of component failure was based on the weakest-link failure theory formulated with Weibull parameters. The theoretical basis is presented in Appendix A. According to the weakest-link theory, failure of a component is triggered by unstable propagation of the most dangerous flaw which is inherently contained in that component [8]. According to the LEFM, the most critical flaw is determined by the most unfavourable combination of size a, location x and orientation ω for a given stress field σ. For simplicity, only sharp planar cracks are considered here.

Random orientation of cracks and multi-axial stress fields necessarily cause a mixed-mode crack tip loading.

In practice, mixed-mode fracture criteria are formulated as an effective criterion in terms of an equivalent mode I stress intensity factor [9,10]. Usually, different mixed-mode criteria will predict different failure risks. We used various mixed-mode effective fracture criteria which were already implemented in STAU (see Appendix B). These were

1. The co-planar energy release rate criterion (co-planar G) [11].
2. The normal stress criterion (normal stress) [12].
3. The maximum hoop stress criterion (hoop stress) [13].
4. The maximum energy release rate criterion (max. G) [14].

4. Weibull parameters of tungsten

In order to obtain the input material data required for the STAU analysis, the Weibull parameters of a commercial tungsten product were experimentally determined. Warm rolled (cross-rolling at 350 °C) tungsten sheets were used for the specimen preparation. For comparison, heat-treated specimens were also tested. Heat-treatment was done at 1000 °C in vacuum for 10 h. Strength data were obtained from four-point bending tests at room temperature. The specimens were prepared using the wire-spark-erosion cutting method. The quality of the machining was controlled by microscopical inspection. The dimension of the specimens was $50\times5\times1$ mm^3. The distance between the inner supports was 20 mm whereas that of the outer supports was 40 mm.

The measured Weibull plots of tungsten strength data are presented in Fig. 2 for the two specimen sets. Both plots showed that the data scattering definitely obeyed a 2-parameter Weibull distribution. The estimated Weibull parameters are given in Table 2. It is noted that the magnitude of the shape parameter (Weibull modulus) was significantly increased by a high-temperature annealing. These data are valid only for un-irradiated or at most slightly irradiated tungsten. As there are no available data yet for the Weibull parameters of irradiated tungsten, several fictitious Weibull parameters were assumed for a parametric study to estimate the effect of embrittlement on the failure probability. The assumed hypothetical shape parameters were 5, 10, 15 and 20. The hypothetical scale parameters were 1500, 2000 and 2500 MPa.

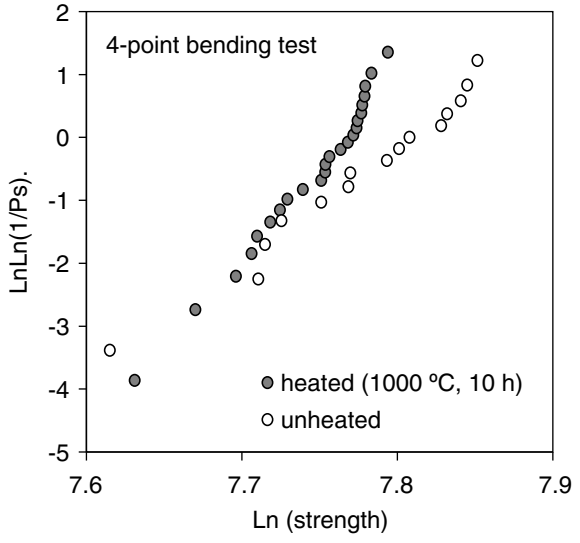

Fig. 2. Weibull plot of tungsten strength data obtained from four-point bending test (open circle: warm rolled at 350°C, solid circle: heat-treated at 1000 °C for 1 h).

Table 2
Measured Weibull parameters

	Shape parameter m	Scale parameter b (MPa)
As-received (warm rolled at 350 °C)	19	2489
Heat-treated (1000 °C, 10 h)	31	2353

5. Results obtained with experimental data

5.1. Stress distributions

In Fig. 3, the residual stress fields of the tungsten block and the subsequent thermal stress fields produced during the heat flux loading are presented (the cooling tube is not displayed). The plots indicate the three normal stress components computed for the reference coordinate system as illustrated in Fig. 1. It is found that the most critical regions are the narrow strip-shaped domains near the free surface edges of the bond interfaces between the tungsten block and the copper alloy tube. The stresses were strongly concentrated in these domains. This feature is a consequence of the well known interfacial stress singularity effect which is usually observed at the free surface edge of a bond interface, when the difference of elastic properties is substantial. The generic fracture mechanical form of the interfacial stress singularity is expressed as a singular function of the radial position r [15]:

$$\sigma_{ij}(r) \propto K \cdot r^{-\omega}, \tag{1}$$

where K is a coefficient (stress intensity factor) and ω is the singularity exponent. ω is a measure of the strength of singular fields and is controlled by the mismatch of elastic constants between two bond partners. The estimated value of ω for the tungsten-copper pair was 0.108 [16].

For each block plate, there are two stress concentration domains on both free surface sides. It is expected that failure of the PFC will be primarily initiated in this domain. The multi-axial nature of the singular stress fields suggests again the necessity of a mixed-mode fracture criterion.

5.2. Failure probability estimated with experimental data

The distribution of local risk of fracture during the heat flux loading is plotted in Fig. 4 in an arbitrary colour scale.

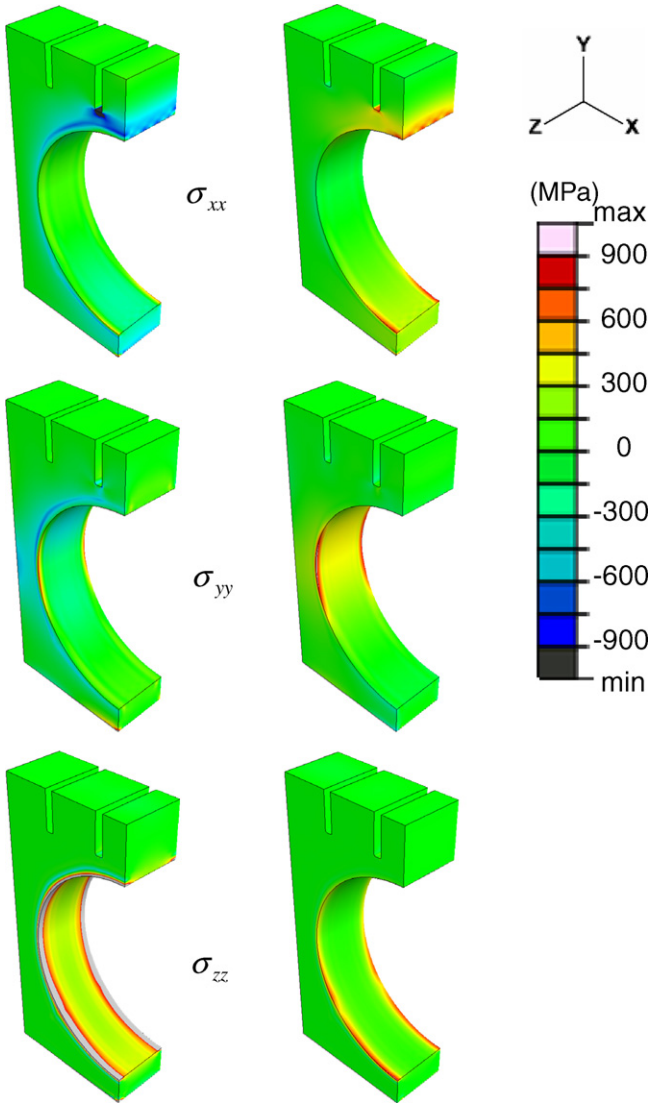

Fig. 3. Residual stresses (left) and thermal stresses during heat flux loading (right) of the tungsten mono-block computed from a FEM simulation. The stress components are presented for the global Cartesian coordinate system. (The heat sink tube is not included in the plots above).

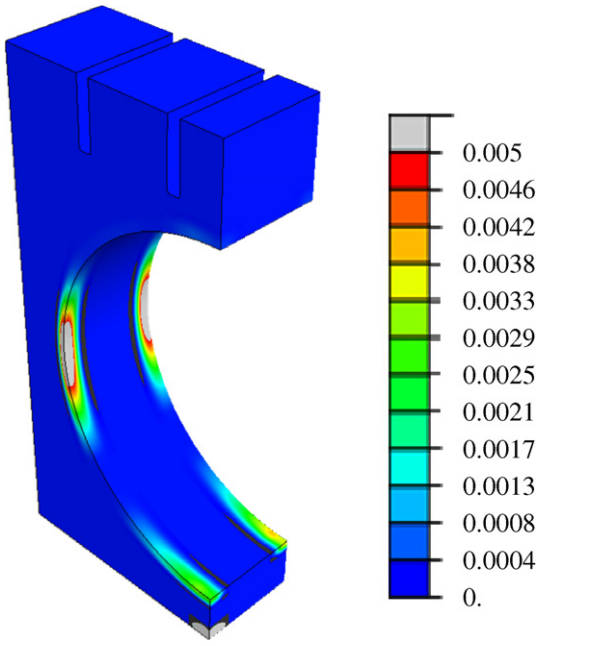

Fig. 4. Distribution of the local risk of fracture illustrated in an arbitrary colour scale. This is the failure probability density estimated for the unit volume associated with each FEM node point.

Table 3
Failure probabilities estimated for surface cracks

m	b	Criterion	σ_0 (MPa)	$P_{F,A}$ (%) (residual)	$P_{F,A}$ (%) (heat load)
19*	2489	Co-planar G	2907	0.024	0.024
		Normal stress	2856	0.026	0.026
		Hoop stress	3097	0.013	0.013
		Max. G	3068	0.015	0.015
31*	2353	Co-planar G	2566	0.007	0.007
		Normal stress	2537	0.007	0.007
		Hoop stress	2705	0.003	0.003
		Max. G	2681	0.003	0.003
5**	1500	Normal stress	2955	25.61	27.05
	2000		3940	6.78	7.21
	2500		4925	2.28	2.42
10**	1500		2019	44.64	44.83
	2000		2692	3.28	3.29
	2500		3365	0.36	0.36
15**	1500		1801	79.70	79.74
	2000		2401	2.11	2.11
	2500		3002	0.08	0.08
20**	1500		1707	99.34	99.34
	2000		2276	1.58	1.58
	2500		2845	0.02	0.02

** Hypothetical parameters.
* Measured parameters.

This distribution illustrates relative risk of local fracture which was computed as a failure probability density at individual FEM nodes [7]. Thus the data values themselves do not give any direct quantitative indication for the failure probability but rather identify the regions of higher local failure risk. The total failure probability data presented in Tables 3 and 4 are the volume integral of this failure probability density field over the whole component domain. As already anticipated from the foregoing stress analysis, the highest risk of local fracture appeared near the free surface edges of the bond interfaces between the tungsten armour and the copper tube.

The results of probabilistic failure analysis obtained using the experimentally estimated data are summarised in Table 3 for surface cracks and in Table 4 for volume cracks. For comparison, four failure probability values are listed estimated with four different mixed-mode fracture criteria. The predicted failure probability ranged from 0.003% to 0.08%. The failure probability of volume cracks was by several factors larger than that of surface cracks.

Table 4
Failure probabilities estimated for volume cracks

m	b	Criterion	σ_o (MPa)	$P_{F,A}$ (%) (residual)	$P_{F,A}$ (%) (heat load)
19*	2489	Co-planar G	2280	0.058	0.058
		Normal stress	2134	0.079	0.079
		Hoop stress	2618	0.057	0.057
		Max. G	2548	0.052	0.052
31*	2353	Co-planar G	2163	0.038	0.038
		Normal stress	2046	0.073	0.073
		Hoop stress	2453	0.035	0.035
		Max. G	2394	0.029	0.029
5**	1500	Normal stress	1463	21.18	24.37
	2000		1951	5.49	6.41
	2500		2438	1.83	2.15
10**	1500		1294	50.27	50.39
	2000		1725	3.86	3.87
	2500		2157	0.42	0.42
15**	1500		1282	95.74	95.75
	2000		1709	4.13	4.13
	2500		2137	0.15	0.15
80**	1500		1287	99.99	99.99
	2000		1716	5.21	5.21
	2500		2145	0.06	0.06

** Hypothetical parameters.
* Measured parameters.

Hence, volume cracks will have a higher contribution to failure than surface cracks. No sensible difference in the failure probability was found between the residual stress state and the heat flux loading state (compare the failure probabilities in the table columns 'residual' and 'heat load'). This rather surprising result could be attributed to the fact that the overall failure risk is governed by the most dangerous domain where stress concentration appears. In the present case stress concentration occurred at the identical locations during the whole stress history, namely, at the free surface edges of the bond interface between the tube and the block. The intensity of the stress concentration in these regions was comparable in both stress states giving a comparable impact on the failure probability. Each failure prediction was notably dependent on which one of the fracture criteria was employed for it. The most conservative estimation was produced by the normal stress criterion. In the case of volume cracks, the three other criteria predicted nearly equal failure probability.

5.3. Failure probability estimated with hypothetical parameters

The results obtained using the hypothetical parameters are summarised also in Table 3 for surface cracks and in Table 4 for volume cracks. The listed data were computed with the normal stress criterion, because it produced the most conservative estimation. Twelve failure probability values were compared corresponding to twelve different combinations of the assumed Weibull parameters. The results showed a trend that in the low strength case ($b < 1500$ MPa) the failure probability was very high ranging from 25% ($m = 5$) to 99% ($m = 20$). When the strength was reduced moderately ($b = 2000$ MPa), the failure probability ranged from 1.6% ($m = 20$) to 7.2% ($m = 5$) for surface cracks whereas it ranged from 3.9% ($m = 10$) to 6.4% ($m = 5$) for volume cracks. The acceptable failure rate was obtained only for the combination of high strength ($b = 2500$ MPa) and just moderately reduced modulus ($m = 20$). In this case the failure probability ranged from 0.02% (surface cracks) to 0.06% (volume cracks).

The results of this parametric study clearly demonstrate the essential impact of possible embrittlement on brittle failure behaviour: a decrease of the scale parameter will lead to an extremely strong increase in the failure risk whereas a decrease of the shape parameter will cause a relatively moderate increase in the failure risk which will be still unacceptably high. The brittle failure response was fairly sensitive to the change of the Weibull parameters.

6. Summary

In this work, we performed the probabilistic failure analysis for a water-cooled tungsten mono-block divertor component to estimate the failure risk of tungsten armour using the STAU code. For the FEM stress analysis, a heat flux load of 15 MW/m^2 and a coolant temperature of 320 °C were assumed. The failure probability was computed according to four different mixed-mode fracture criteria.

Both experimental and hypothetical Weibull parameters were used as material data. The measured shape parameters were 19 (as-received) and 31 (heat-treated) and the measured scale parameters were 2489 (as-received) and 2353 MPa (heat-treated). The assumed hypothetical shape parameters used for the parametric study were 5, 10, 15 and 20 and the hypothetical scale parameters were 1500, 2000 and 2500 MPa.

In the case of unirradiated tungsten, the failure probability was acceptably small ranging from 0.025% (surface cracks) to 0.08% (volume cracks). When either the Weibull modulus or the scale parameter was hypothetically reduced, the resulting failure risk was significantly increased. This result clearly demonstrates the essential impact of embrittlement on the brittle failure behaviour of the water-cooled tungsten mono-block divertor.

Acknowledgements

The authors are grateful to Mr Martin Härtelt, IMF II, Forschungszentrum Karlsruhe, Germany, for his support and valuable discussions.

Appendix A. Weibull theory of brittle failure [7]

In STAU, volume flaws and surface flaws are modelled as penny-shaped cracks and through-wall cracks,

respectively. The singular crack tip stress fields under mixed-mode loads are expressed in terms of the stress intensity factors K corresponding to three fracture modes:

$$K_{\mathrm{I}} = \sigma_n Y_{\mathrm{I}} \sqrt{a}, \quad K_{\mathrm{II}} = \tau_{\mathrm{II}} Y_{\mathrm{II}} \sqrt{a}, \quad K_{\mathrm{III}} = \tau_{\mathrm{III}} Y_{\mathrm{III}} \sqrt{a}, \quad \text{(A.1)}$$

where Y denotes geometric correction factor and σ and τ the projections of the stress tensor on the crack plane which are computed by the tensor transformation rules.

The mixed-mode failure criterion for a multi-axial stress field has a generic form

$$g(\sigma_n, \tau_{\mathrm{II}}, \tau_{\mathrm{III}}) \geqslant g_{\mathrm{c}} \quad \text{(A.2)}$$

In STAU, the effective failure criterion is employed which is formulated with equivalent mode I stress intensity factor as follows:

$$g(K_{\mathrm{Ieq}}, 0, 0) = g(K_{\mathrm{I}}, K_{\mathrm{II}}, K_{\mathrm{III}}) \quad \text{(A.3)}$$

Then the failure criterion is reformulated as

$$K_{\mathrm{I\,eq}} \geqslant K_{\mathrm{I\,c}}, \quad \text{(A.4)}$$

where $K_{\mathrm{I\,c}}$ stands for the mode I fracture toughness.

By analogy to Eq. (1), an equivalent stress σ_{eq} is defined by

$$K_{\mathrm{I\,eq}} \equiv \sigma_{\mathrm{eq}} Y_{\mathrm{I}} \sqrt{a} \quad \text{(A.5)}$$

Finally, the critical crack size a_{c} is given by

$$a_{\mathrm{c}} = \left(\frac{K_{\mathrm{I\,c}}}{\sigma_{\mathrm{eq}} Y_{\mathrm{I}}} \right)^2 \quad \text{(A.6)}$$

Failure by spontaneous crack extension occurs if the crack size a exceeds a_{c}.

As the size, the location and the orientation are random variables, the strength is also a random variable for which a statistical treatment is required. For statistically independent infinitesimal volume elements $\mathrm{d}V$ the actual number n of cracks contained in a component is a Poisson distributed random variable.

The probability density function of the crack size a is expressed by a Pareto distribution by

$$f_a(a) = 1 - \frac{a_0^{r-1}}{a^{r-1}} \quad \text{(A.7)}$$

where $a \geqslant a_0$.

For a multi-axially loaded brittle component containing randomly oriented sharp volume cracks of an arbitrary (large) number, the failure probability due to the unstable crack propagation is formulated as

$$P_{F,V} = 1 - \exp\left[-\frac{1}{V_0} \int_V \frac{1}{4\pi} \int_\Omega \left(\frac{\sigma_{\mathrm{eq}}(x,\omega)}{\sigma_0} \right)^m \mathrm{d}\Omega \mathrm{d}V \right] \quad \text{(A.8)}$$

where V_0 is the unit volume containing an average number of M_0 cracks. m and σ_0 are material parameters expressed as

$$m = 2(r-1) \quad \text{(A.9)}$$

$$\sigma_0 = \frac{1}{(M_0)^{\frac{1}{m}}} \cdot \frac{K_{\mathrm{I\,c}}}{Y_I \sqrt{a_0}} \quad \text{(A.10)}$$

Further, Eq. (A.8) can be rewritten in terms of a 2-parameter Weibull distribution:

$$P_{F,V} = 1 - \exp\left[-\left(\frac{\sigma^*}{b} \right)^m \right] \quad \text{(A.11)}$$

where σ^* denotes a reference stress characterising the load level.

The Weibull parameter b is related to σ_0 by

$$b = \sigma_0 \left[\frac{1}{V_0} \int_V \frac{1}{4\pi} \int_\Omega \left(\frac{\sigma_{\mathrm{eq}}(x,\omega)}{\sigma^*} \right)^m \mathrm{d}\Omega \mathrm{d}V \right]^{-\frac{1}{m}} \quad \text{(A.12)}$$

Eqs. (A.11) and (A.12) suggest that the required parameters m and σ_0 can be obtained from a series of uniaxial tests where the shape parameter m and the scale parameter b are estimated from the measured strength data of simple specimens using the Weibull statistics. At the stage of parameter calibration the effective stress in Eq. (A.12) refers to the stress state produced by the testing.

In the case of surface cracks of the length $2a$ normal to the surface, the failure probability $P_{F,A}$ of a component containing arbitrary number of randomly oriented sharp surface cracks of random size and random location is given in the same line as $P_{F,V}$:

$$P_{F,A} = 1 - \exp\left[-\frac{1}{A_0} \int_V \frac{1}{2\pi} \int_\Omega \left(\frac{\sigma_{\mathrm{eq}}(x,\omega)}{\sigma_0} \right)^m \mathrm{d}\Omega \mathrm{d}A \right] \quad \text{(A.13)}$$

Then the Weibull parameter b is related to σ_0 by

$$b = \sigma_0 \left[\frac{1}{A_0} \int_A \frac{1}{4\pi} \int_\Omega \left(\frac{\sigma_{\mathrm{eq}}(x,\omega)}{\sigma^*} \right)^m \mathrm{d}\Omega \mathrm{d}A \right]^{-\frac{1}{m}} \quad \text{(A.14)}$$

The domain and the orientation integrals are estimated numerically by means of the Gauss quadrature method for each finite element. To this end, the analytical formulation for $P_{F,V}$ and $P_{F,A}$ has to be converted into a discretised form, for instance:

$$\begin{aligned} P_{F,V} &= 1 - \exp\left[-\frac{1}{V_0} \sum_{e=1}^{N_{\mathrm{e}}} \int_{V_{\mathrm{e}}} \frac{1}{4\pi} \int_\Omega \left(\frac{\sigma_{\mathrm{eq}}(\vec{x},\vec{\omega})}{\sigma_0} \right)^m \mathrm{d}\Omega \mathrm{d}V \right] \\ &= 1 - \exp\left[-\frac{1}{V_0} \sum_{e=1}^{N_{\mathrm{e}}} \int_{-1}^{1} \int_{-1}^{1} \int_{-1}^{1} \frac{1}{4\pi} \int_{-1}^{1} \int_{-1}^{1} \right. \\ &\quad \left. \times \left(\frac{\sigma_{\mathrm{eq}}(\vec{\xi},\vec{\theta})}{\sigma_0} \right)^m J_V(\vec{\xi}) \quad \cdot J_\Omega(\vec{\theta}) \cdot \mathrm{d}\vec{\theta} \cdot \mathrm{d}\vec{\xi} \right] \end{aligned} \quad \text{(A.15)}$$

where N_{e} is the number of elements of the FEM model, N_{e} the volume of the eth element, N_{e} and N_{e} are the coordinates in the reference configuration considered for the numerical integration using the Gauss quadrature and J_V and J_Ω denote Jacobians of the corresponding variable transformations.

Appendix B. Equivalent stress and effective fracture criteria [7]

(1) The co-planar energy release rate criterion [11]

$$K_{\mathrm{I\,eq}} = \left[K_{\mathrm{I}}^2 + K_{\mathrm{II}}^2 + \frac{1}{1-v}K_{\mathrm{III}}^2\right]^{0.5} \tag{B.1}$$

$$\sigma_{\mathrm{eq}} = \left[\sigma_{\mathrm{I}}^2 + \tau_{\mathrm{II}}^2\left(\frac{Y_{\mathrm{II}}}{Y_{\mathrm{I}}}\right)^2 + \frac{\tau_{\mathrm{III}}^2}{1-v}\left(\frac{Y_{\mathrm{III}}}{Y_{\mathrm{I}}}\right)^2\right]^{0.5} \tag{B.2}$$

(2) The normal stress criterion [12]

$$K_{\mathrm{I\,eq}} = K_{\mathrm{I}} \tag{B.3}$$

$$\sigma_{\mathrm{eq}} = \sigma_n \tag{B.4}$$

(3) The maximum hoop stress criterion [13]

$$K_{\mathrm{I\,eq}} = \frac{\sqrt{8}\left[2K_{\mathrm{I}} + 6\sqrt{K_{\mathrm{I}}^2 + 8K_{\mathrm{II}}^2}\right]K_{\mathrm{II}}^3}{[K_{\mathrm{I}}^2 + 12K_{\mathrm{II}}^2 - K_{\mathrm{I}}\sqrt{K_{\mathrm{I}}^2 + 8K_{\mathrm{II}}^2}]^{1.5}} \tag{B.5}$$

$$\sigma_{\mathrm{eq}} = \frac{\sqrt{8}\left[2\sigma_n + 6\sqrt{\sigma_n^2 + 8\tau_{\mathrm{II}}^2(Y_{\mathrm{II}}/Y_{\mathrm{I}})^2}\right]\tau_{\mathrm{II}}^3(Y_{\mathrm{II}}/Y_{\mathrm{I}})^3}{\left[\sigma_n^2 + 12\tau_{\mathrm{II}}^2(Y_{\mathrm{II}}/Y_{\mathrm{I}})^2 - \sigma_n\sqrt{\sigma_n^2 + 8\tau_{\mathrm{II}}^2(Y_{\mathrm{II}}/Y_{\mathrm{I}})^2}\right]^{1.5}} \tag{B.6}$$

(4) The maximum energy release rate criterion [14]

$$K_{\mathrm{I\,eq}} = \left[K_{\mathrm{I}}^4 + 6K_{\mathrm{I}}^2K_{\mathrm{II}}^2 + K_{\mathrm{II}}^4\right]^{0.25} \tag{B.7}$$

$$\sigma_{\mathrm{eq}} = \left[\sigma_n^4 + 6\sigma_n^2\tau_{\mathrm{II}}^2(Y_{\mathrm{II}}/Y_{\mathrm{I}})^2 + \tau_{\mathrm{II}}^4(Y_{\mathrm{II}}/Y_{\mathrm{I}})^4\right]^{0.25} \tag{B.8}$$

References

[1] H. Bolt, V. Barabash, W. Krauss, J. Linke, R. Neu, S. Suzuki, N. Yoshida, ASDEX Upgrade Team, J. Nucl. Mater. 329–333 (2004) 66.

[2] N. Baluc, Assessment report on W, Final report on EFDA task TW1-TTMA-002 Deliverable 5, 2002.

[3] Y. Ishijima, H. Kurishita, K. Yubuta, H. Arakawa, M. Hasegawa, Y. Hiraoka, T. Takida, K. Takebe, J. Nucl. Mater. 329–333 (2004) 775.

[4] D. Maisonnier et al., A conceptual study of commercial fusion power plants, final report of the European Fusion Power Plant Conceptual Study (PPCS) EFDA-RP-RE-5.0, 2005.

[5] ABAQUS 6.6 User's manual Analysis, ABAQUS Inc., Providence RI, 2006.

[6] ITER Material Properties Handbook (IMPH), ITER Document No. S74 RE1 and G74 MA16, 2005.

[7] A. Brückner-Foit, A. Heger, K. Heiermann, P. Hülsmeier, A. Mahler, A. Mann, Ch. Ziegler, STAU 4 User's manual, Forschungszentrum Karlsruhe, Karlsruhe, 2003.

[8] S.B. Batdorf, H.L. Heinisch, J. Am. Ceram. Soc. 61 (1978) 355.

[9] T. Thiemeier, A. Brückner-Foit, H. Kölker, J. Am. Ceram. Soc. 74 (1991) 48.

[10] D. Munz, T. Fett, Ceramics: Mechanical Properties, Failure Behaviour, Materials Selection, Springer-Verlag, Berlin, Heidelberg, 1999.

[11] P.C. Paris, G.C. Sih, Am. Soc. Test. Mater., Philadelphia, ASTM STP 381, 1965, p. 30.

[12] D. Broek, Elementary Engineering Fracture Mechanics, 4th Ed., Martinus Nijhoff Publishers, Dordrecht, 1986.

[13] F. Erdogan, G.C. Sih, J. Basic Eng. 85 (1963) 519.

[14] T.K. Hellen, W.S. Blackburn, Int. J. Fracture 11 (1975) 605.

[15] D.B. Bogy, Trans. ASME J. Appl. Mech. 35 (1968) 460.

[16] J.H. You, H. Bolt, J. Nucl. Mater. 299 (2001) 1.